Available online at www.sciencedirect.com

SciVerse ScienceDirect

Ceramics International 38 (2012) 5355–5361

CERAMICS INTERNATIONAL

www.elsevier.com/locate/ceramint

# Enhanced sinterability of mechanical alloyed $La_{9.33}Si_2Ge_4O_{26}$ oxyapatite powders for IT-SOFC electrolytes

R. Serra [a], C. Alves [b], F.A.C. Oliveira [b], T. Marcelo [b], J. Mascarenhas [b], B. Trindade [a,*]

[a] CEMUC, Mechanical Engineering Department, University of Coimbra, Rua Luís Reis Santos, 3030-788 Coimbra, Portugal

[b] Laboratório Nacional de Energia e Geologia I.P., Product Engineering Unit, Estrada do Paço do Lumiar, 1649-038 Lisboa, Portugal

Received 7 February 2012; received in revised form 15 March 2012; accepted 16 March 2012

Available online 30 March 2012

**Abstract**

Dense oxyapatite-based $La_{9.33}Si_2Ge_4O_{26}$ electrolytes have been successfully prepared by electrical sintering at 1400 °C in static air for 1 h from dry milling $La_2O_3$, $SiO_2$ and $GeO_2$ powders, in adequate atomic proportions, at 350 rpm for 15 h, under controlled environmental conditions, in a planetary ball mill. The densification behaviour of apatite-type phase $La_{9.33}Si_2Ge_4O_{26}$ powders synthesized by mechanical alloying was investigated through microstructural evolution with sintering temperature by means of XRD and SEM/EDS analyses. The content of germanium in the sintered samples remained almost constant, suggesting that its incorporation in the apatite phase hinders the high temperature (>1250 °C) volatilization process.



*Keywords:* A. Sintering; Lanthanum-based oxyapatite; Mechanical alloying; SOFC

## 1. Introduction

Oxide ion conducting materials are being considered for a range of technological applications, such as electrolytes in solid oxide fuel cells (SOFCs). One of the key components of SOFC, in terms of high cell efficiency, low manufacturing cost and increased long-term operation stability, is the solid electrolyte. An electrolyte must possess high oxide ion conductivity (typically $>1 \times 10^{-3}$ S cm$^{-1}$), low electronic conductivity, good thermal shock resistance and chemical stability, in both reducing and oxidizing environments, as well as gas impermeability and compatibility (both chemical and thermal) with the electrodes [1]. Several technical problems still need to be overcome before SOFC commercialization becomes a reality, and so the development of new materials with improved properties is of upmost importance. In particular, the development of new oxide ion conductors with improved performance and durability is sought. Nowadays electrolytes based on yttria-stabilized zirconia (YSZ), which exhibits high ionic conductivity at elevated temperatures (850–1000 °C), are widely used in spite of their problems of cell sealing and lifetime. To increase components durability lowering SOFC operating temperatures is required. One way to achieve such goal would be moving towards increasingly thinner YSZ electrolyte, but this is not an optimal solution. Hence, other materials are being investigated to replace YSZ, and significant research work has been conducted on the apatite-type oxide phases, such as M-doped lanthanum oxides of general formula $La_{10}(MO_4)_6O_2$ where M is an element, such as Ge, Si, Al or P. These oxides exhibit high ionic conductivity and low activation energy at moderate temperatures (500–750 °C) when compared to YSZ electrolyte [2]. Their structure consists of isolated $MO_4$ tetrahedra with the La cations located in two cavity sites, one 7 coordinate and one 9 coordinate. The extra oxygen anions occupy channels running through the structure. These oxide ion channels are presumed to be responsible for the high ionic conductivity of such oxyapatite phases [3]. It is also known that ion conductivity can be further improved with lanthanum deficiency, the maximum deviation from stoichiometric composition depending on the system considered [4].

One of the main limitations of oxyapatite materials manufacture is related to their poor sinterability [5]. Several efforts are being made for obtaining apatite materials through different routes, such as solid state reaction [2], sol–gel

* Corresponding author. Tel.: +351 239790794.
*E-mail address:* bruno.trindade@dem.uc.pt (B. Trindade).

0272-8842/$36.00 
doi:10.1016/j.ceramint.2012.03.042

synthesis [6], hot-pressing [7], mechanical milling [8], precipitation combined with an azeotropic-distillation process [9], colloidal processing [10] and floating zone methods [11]. Various problems in processing such apatite materials, as very thin gastight electrolytes, were encountered and have been recently reviewed [12,13]. Poor control of grain morphology, grain growth and $GeO_2$ volatilization above ~1300 °C [14–16] require careful consideration, as well as other key properties rather than just the high ionic conductivity need to be optimized such as thermo-mechanical properties. In this context, mechanical alloying (MA) is regarded as a potential alternative processing method to obtain apatite-like lanthanum oxide conductors at reduced costs [7,17,18]. During the MA process, heavy deformation is introduced into the particles, increasing the defect density, which accelerates the diffusion process by decreasing the diffusion distances. Therefore, sintering of these highly disordered materials can be achieved at lower temperatures than that required by conventional routes (typically >1600 °C). The main drawbacks of MA are (a) Fe contamination that can improve sinterability but reduce ionic conductivity [19] and (b) poor chemical homogeneity which may result in formation of unwanted secondary phases with rather low conductivities.

In previous works, Si- and Ge-doped lanthanum oxide materials with apatite-type phase were produced by MA and subsequent annealing [20,21]. A dependence of apatite-type phase formation on the MA parameters was shown, the higher the MA rotation speed and/or processing time, the lower the annealing temperature required for its formation. Under optimized conditions, mixed Si/Ge-based apatite phase could be obtained at 350 rpm for 15 h at room temperature. In the present work, influence of pre-milling the raw powders and mixing them in different atmospheres (either Ar or air) on the densification behaviour of MA powders was investigated in order to obtain a dense single-phase hexagonal apatite-type at moderate temperatures (up to 1400 °C).

## 2. Experimental

All samples were prepared from $La_2O_3$ (99.9%), $SiO_2$ (99.4%) and $GeO_2$ (99.9%) powders from Neyco. Characterization of the raw materials can be found elsewhere [22]. Mixtures with $7La_2O_3$:$3SiO_2$:$6GeO_2$ molar ratios were used in order to obtain the $La_{9.33}Si_2Ge_4O_{26}$ phase. The blends were mechanically alloyed at 350 rpm for 15 h in a Fritsch planetary ball mill using a 250 ml hardened steel vial and 15 balls with 20 mm diameter of the same material. About 25 g of the powder blend was loaded into the vial to get a ball-to-powder weight ratio of 20:1. Some of the experiments were carried out under protective atmosphere (argon at 200 kPa), the remaining being performed under atmospheric air. The powders were mechanically alloyed either in the as-received condition or after milling the starting materials separately at 350 rpm for 10 and 30 min in argon at 50 kPa (hereafter referred to as ''pre-milled condition''). With this procedure, it was expected to promote apatite phase formation as well as to achieve a particle size distribution suitable to obtain high green densities in the subsequent compaction.

The blends were compacted either by cold isostatic pressing (CIP) at 300 MPa or by uniaxial pressing at 393 and 620 MPa followed by sintering for 1 h at temperatures in the range 1300–1400 °C under static air in an electrical furnace (model SF2, Sater S.A., Spain) with $MoSi_2$ heating element. The heating and cooling rates were set at 5 °C $min^{-1}$. The experimental conditions used for the manufacturing are compiled in Table 1.

The geometric density (weight/volume) of the green compacted samples was measured. For the sintered samples, density and open porosity were determined using the boiling test method [23].

After mechanical alloying, the mean particle size and particle size distribution of the mixtures were measured by laser scattering (CILAS 1064); the mixtures were also analysed by X-ray diffraction (XRD, Philips X'Pert PW 3020). The sintered samples were characterized by XRD as well as by Scanning Electron Microscopy with Electron Dispersive Spectrometry (SEM/EDS, Philips XL30/EDAX and XL30FEG/EDAX), carried out on mounted and polished surfaces, coated with a thin layer of Au–Pd to provide surface electrical conductivity (Sputter Coater Emitech K575X).

XRD measurements were also performed using $CoK_\alpha$ radiation ($\lambda$ = 1.78897 Å) within the $2\theta$ range of 20–40° using a step size of 0.02° ($2\theta$) and an acquisition time of 2 s per step. Phase identification was carried out with reference to the ICDD cards database, using the X'Pert dedicated software.

Quantification of the iron contamination resulting from the milling process was assessed by PIXE analysis carried out on some sintered samples at the nuclear microprobe facility of ITN – Nuclear Technology Institute, which is located on a 3.1 MV single-ended Van de Graaff accelerator, using a 2.0 MeV focused proton beam of 2.6 mm × 2.6 mm, according to the procedure described in detail elsewhere [24].

Table 1
Samples identification and experimental conditions used for their fabrication.

| Sample identification | Pre-milling time (min) | MA atmosphere | Compaction/pressure (MPa) | Sintering temperature (°C) |
|---|---|---|---|---|
| S1 | 30 | Argon | Uniaxial/393 | 1300 |
| S2 | 30 | Argon | Uniaxial/393 | 1350 |
| S3 | 30 | Argon | Uniaxial/393 | 1400 |
| S4 | 0 | Air | CIP/300 | 1400 |
| S5 | 30 | Air | Uniaxial/620 | 1400 |
| S6 | 10 | Air | Uniaxial/620 | 1400 |

## 3. Results and discussion

### 3.1. Powder mixtures characterization

Fig. 1 shows the influence of pre-milling the raw materials on the particle size distributions of the mechanically alloyed mixtures. The characteristic particle diameters $d_{10}$, $d_{50}$ and $d_{90}$ of all the mixtures are summarized in Table 2.

As can be seen from Fig. 1, the size distributions are multimodal, the curves having a similar shape. However, the particle sizes decreased as a consequence of pre-milling the starting powders and the lowest values were obtained from powders pre-milled for 10 min. The values from sample S5 (30 min) are larger than that of sample S6, which can be attributed to agglomeration, since finer powders are likely to form agglomerates.

Fig. 2 shows the XRD patterns of the mechanically alloyed mixtures and diffraction data [25] of the apatites $La_{9.33}Si_6O_{26}$ (ICDD card no. 49-0443) and $La_{9.36}Si_3Ge_3O_{26}$ (ICDD card no. 75-3458); no ICDD card is available for the composition of the present work. The diffraction peaks of those samples are shifted to lower angles (higher interplanar distances) when compared to that indicated for the apatite $La_{9.33}Si_6O_{26}$. This is the result of the larger size of the Ge atom when compared to the Si one. However, the peak positions match better with the Ge-doped apatite $La_{9.36}Si_3Ge_3O_{26}$. The hexagonal lattice parameters and unit cell volume of the apatite phase formed during mechanical alloying (MA) of the mixtures are shown in Table 3 together with values taken from the ICDD cards 49-0443 and 75-3458 for comparison. The *a* parameter of all samples is higher than the values reported in the ICCD cards of both apatites. The calculated *c* parameters are similar to that reported for the $La_{9.36}Si_3Ge_3O_{26}$ phase and higher than that of the $La_{9.33}Si_6O_{26}$ phase. As reported in a previous work [21], this confirms the presence of the Ge atoms in the Si/Ge-O tetrahedral sites of the apatite phase. Increase of the lattice parameters can be explained by the slightly higher ionic radius of the germanium ion (0.67 Å for $Ge^{4+}$ and 0.54 Å for $Si^{4+}$). The *a* direction is more sensitive to the substitution of Si for Ge atoms [2], giving rise to a distortion of the apatite unit cell. In fact, taking into account the two ICDD cards of the apatite phase with and without Ge, it can be seen that replacement of 50% of Si atoms for Ge atoms leads to a negative variation of the *c/a* ratio of 0.4%.

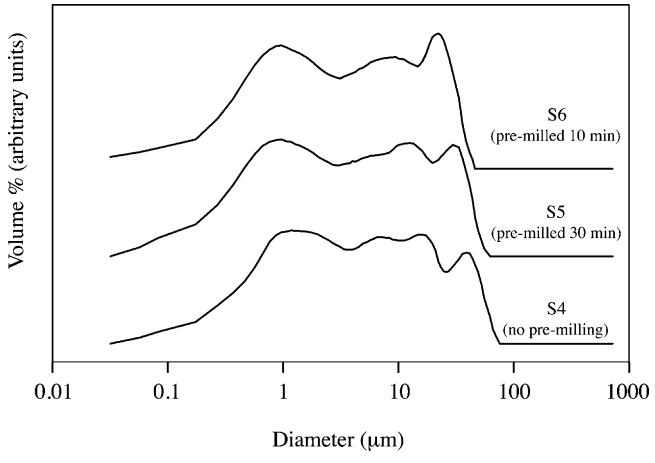


Fig. 1. Particle size distribution of the mixtures mechanically alloyed in air, as a function of the raw materials pre-milling.

Table 2
Characteristic particle diameters of the mechanically alloyed mixtures.

| Sample identification | $d_{10}$ (μm) | $d_{50}$ (μm) | $d_{90}$ (μm) |
|---|---|---|---|
| S1 (=S2 = S3) | 0.38 | 3.30 | 28.57 |
| S4 | 0.38 | 3.12 | 24.74 |
| S5 | 0.30 | 2.55 | 21.42 |
| S6 | 0.26 | 2.28 | 17.88 |

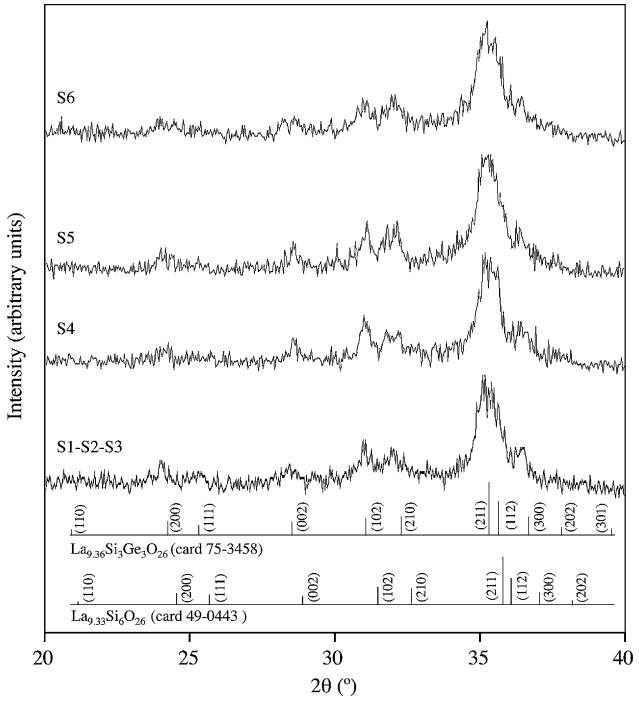


Fig. 2. XRD patterns of the mechanically alloyed mixtures.

### 3.2. Sintering

Measured green and sintered densities, as well as open porosities of the sintered samples are summarized in Table 4.

Table 3
Lattice parameters and unit cell volume of the apatite formed during MA.

| Sample identification | *a* (Å) | *c* (Å) | *c/a* | Volume (Å$^3$) $3a^2 \sin 60°c$ |
|---|---|---|---|---|
| S1 (=S2 = S3) | 9.90 | 7.27 | 0.734 | 1850 |
| S4 | 9.92 | 7.25 | 0.731 | 1853 |
| S5 | 9.93 | 7.26 | 0.731 | 1859 |
| S6 | 9.96 | 7.25 | 0.728 | 1868 |
| $La_{9.36}Si_3Ge_3O_{26}$ ICDD 75-3458 | 9.86 | 7.27 | 0.737 | 1836 |
| $La_{9.33}Si_6O_{26}$ ICDD 49-0443 | 9.71 | 7.19 | 0.740 | 1761 |

Samples that were sintered at 1400 °C (S3–S6) have higher density and, consequently, lower porosity than the samples sintered at 1300 and 1350 °C (S1 and S2, respectively). No density data could be found for Ge/Si doped apatites; however, the density of 5.517 g cm$^{-3}$ of the apatite $La_{9.36}Si_3Ge_3O_{26}$ calculated from its unit cell volume [25], can be taken as a reference value for the density of the materials produced in the present work and, accordingly, S3 is almost fully dense (98% of the reference). Nevertheless, the values of sintered density obtained in this work, with exception of S1 (1300 °C) are higher than those reported in the literature for $La_{9.33}Si_6O_{26}$ electrolytes sintered at 1500 °C for 4 h (4.89–5.04 g cm$^{-3}$) [26]. However, bulk densities for $La_{10}Si_6O_{27}$ electrolytes sintered at 1550–1650 °C for 4 h in air (4.79–5.30 g cm$^{-3}$, depending upon the synthesis method employed) [27] are more close to those listed in Table 4. It is worth noting that, in general, a temperature of 1700 °C is required to achieve densities of 90–95% using solid-state powder synthesis, whereas at 1500 °C the final density is lower than 83% of the theoretical one [28].

Comparing the samples mechanically alloyed in air, it can be seen that the mixtures prepared from pre-milled powders (S5 and S6) have higher sintered density than that with no pre-milling (S4), so it is evident that pre-milling the raw powders was of upmost importance in achieving higher final densities. However it seems that the sintering temperature has greater influence on the final density than powders pre-milling since S1 (30 min pre-milling, 1300 °C sintering temperature) has a much larger amount of porosity than S4 (no pre-milling, 1400 °C sintering temperature). Apparently, the MA atmosphere has little influence on the sintered density as can be seen when comparing S3 to S5.

Fig. 3 shows the X-ray diffraction patterns of the sintered samples. The spectra are quite similar, consisting mainly of peaks of the apatite phase (ICDD card 75-3458) and other peaks of minor phases, such as $La_4GeO_8$ (ICDD card 040-1185). Some peaks of low intensity, close to $2\theta = 30^\circ$ and 34.5°, could not be identified.

The experimental conditions used do not seem to have a clear effect on the phases formed, the apatite-type structure being the major phase in all samples. However, the *c/a* ratio of the $La_{9.33}Si_2Ge_4O_{26}$ lattice increased during sintering, as can be seen when comparing the values measured on the sintered samples and shown on Table 5 with those of Table 3. In addition, a decrease of the unit cell volume of the lattice is

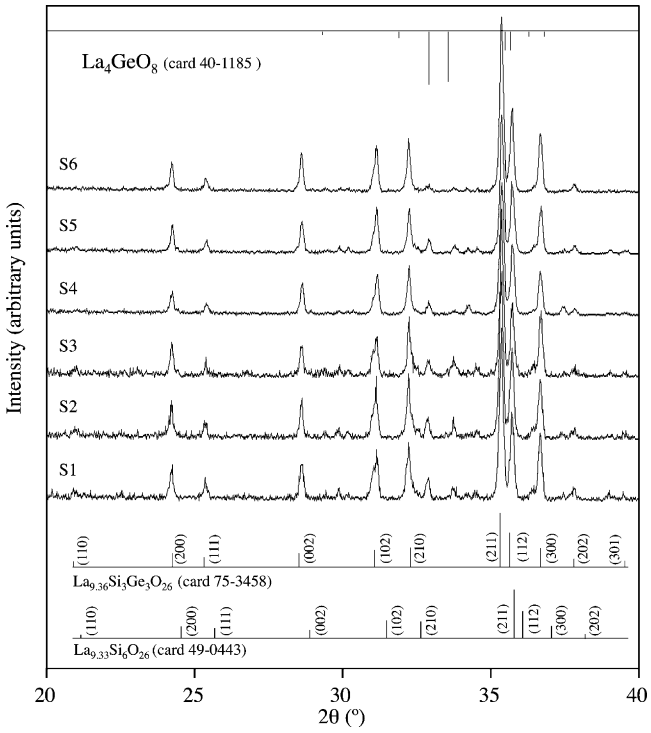


Fig. 3. X-ray diffraction patterns of the sintered samples.

observed. The values obtained tend to reach the ones indicated for the $La_{9.36}Si_3Ge_3O_{26}$ phase. One possible explanation is that the apatite did not remain chemically stable upon sintering and it is possible that some germanium atoms have left the apatite structure to form new structural phases.

As mentioned before, one of the initial concerns of this study was whether or not the germanium atoms would stay in the apatite structure at the necessary sintering high temperatures. To clarify this point, EDS semi-quantitative analysis was carried out at 10 kV. Five EDS measurements (100 μm × 100 μm area analysis) were performed on each sintered sample and the La-Lα, Ge-Lα and Si-Kα peak areas were used to compute the La/(Si+Ge) atomic ratios. The results varied in the range 1.55–1.57, which are comparable to the value of 1.57 calculated for $La_{9.33}Si_2Ge_4O_{26}$ from the theoretical atomic weights. In a work on the oxide ion conductivity of mixed Si/Ge-based apatite-type systems, Sansom et al. [14] claim that Ge volatility increases with increasing Ge content. However, this assumption is based on results of global mass loss of samples (both powders and

Table 4
Green and sintered density of the pellets and open porosity measured on sintered pellets.

| Sample identification | Sintering temperature (°C) | Green density (g cm$^{-3}$) | Sintering density (g cm$^{-3}$) | Open porosity (%) |
|---|---|---|---|---|
| S1 | 1300 | 3.63 | 4.81 | 13.4 |
| S2 | 1350 | 3.68 | 5.13 | 6.15 |
| S3 | 1400 | 3.58 | 5.42 | 1.11 |
| S4 | 1400 | 3.83 | 5.13 | 4.18 |
| S5 | 1400 | 3.79 | 5.36 | 1.80 |
| S6 | 1400 | 3.75 | 5.34 | 2.36 |

Table 5
Lattice parameters and unit cell volume of the apatite after sintering.

| Sample identification | *a* (Å) | *c* (Å) | *c/a* | Volume (A$^3$) $3a^2$ sin 60°c |
|---|---|---|---|---|
| S1 | 9.8386 | 7.2523 | 0.737 | 1823 |
| S2 | 9.8438 | 7.2569 | 0.737 | 1826 |
| S3 | 9.8431 | 7.2512 | 0.737 | 1825 |
| S4 | 9.8426 | 7.2447 | 0.736 | 1822 |
| S5 | 9.8511 | 7.2488 | 0.736 | 1827 |
| S6 | 9.8422 | 7.2491 | 0.737 | 1824 |

pellets) and not directly on chemical quantification of Ge. Nevertheless, prolonged heating of $La_{9.33}Ge_6O_{26}$ at 1500 °C for 120 h has resulted in a transformation into $La_2GeO_5$ due to Ge loss [29].

Taking into account the results of XRD and EDS analyses, one might state that sintering can be the cause of a partial loss of Ge atoms from the apatite phase and this might be the reason for the appearance of other phases than the apatite one, e.g. $La_4GeO_8$. Indeed, germanium is the most volatile element present. However, EDS evidence suggests that Ge is homogenously distributed throughout the samples. Hence, the exact mechanism of the loss of Ge from the apatite phase needs to be further examined. Once incorporated in the apatite phase, it appears that volatilization of Ge at temperatures higher than 1250 °C [29] is prevented, at least for short dwell times (1 h).

No significant iron contamination from the mechanical alloying vial and balls was detected in the sintered samples. PIXE analysis revealed Fe amounts of about 5000 ppm, which is quite acceptable for the synthesis technique used. However, the presence of iron impurities in the apatite should not be a problem, with some authors [30] claiming that iron increases the conductivity of apatite and lowers its densification temperature. However, Jothinathan et al. [6] found that the composition $La_{9.83}Fe_{1.5}Si_{4.5}O_{26}$ prepared using the sol–gel route requires 5 h at 1500 °C for obtaining relative densities higher than 96% by conventional pressureless sintering in air.

Microstructural characterization by SEM of the sintered samples is shown in Fig. 4. The main feature of these microstructures is the presence of porosity resulting mainly from non-densified areas, the amount of porosity decreasing with increasing sintering temperature, in accordance with results shown in Table 4.

Apparently, mixture S3 exhibits the smallest porosity (pore size was not evaluated) most of which resulting from entrapped air; this is in agreement to the reduced amount of open porosity and the highest density measured on this material. Most pores are typically smaller than 10 μm and are mostly round and of closed type indicating that the sintering stage is approaching

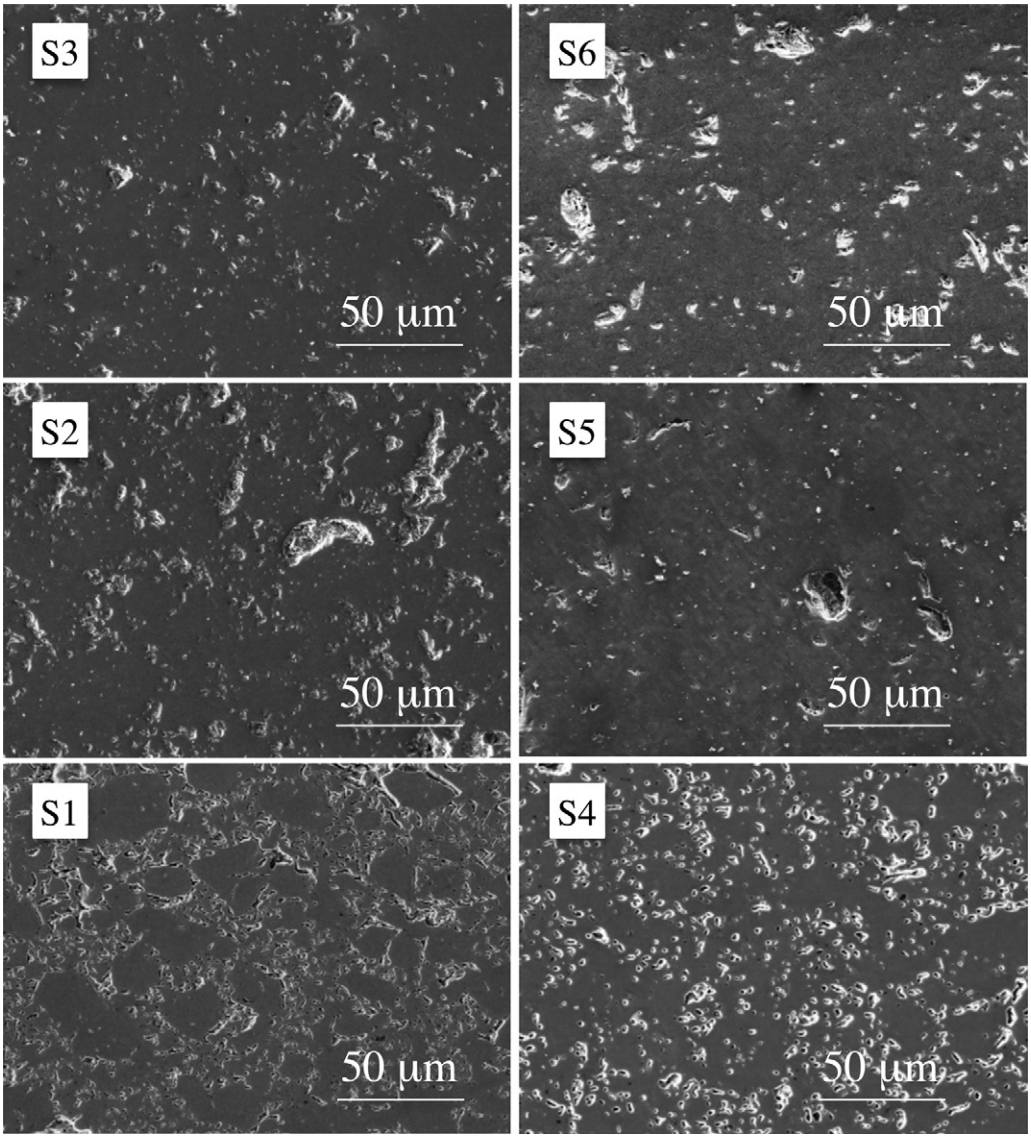


Fig. 4. SEM micrographs (secondary electron images) of the sintered samples.

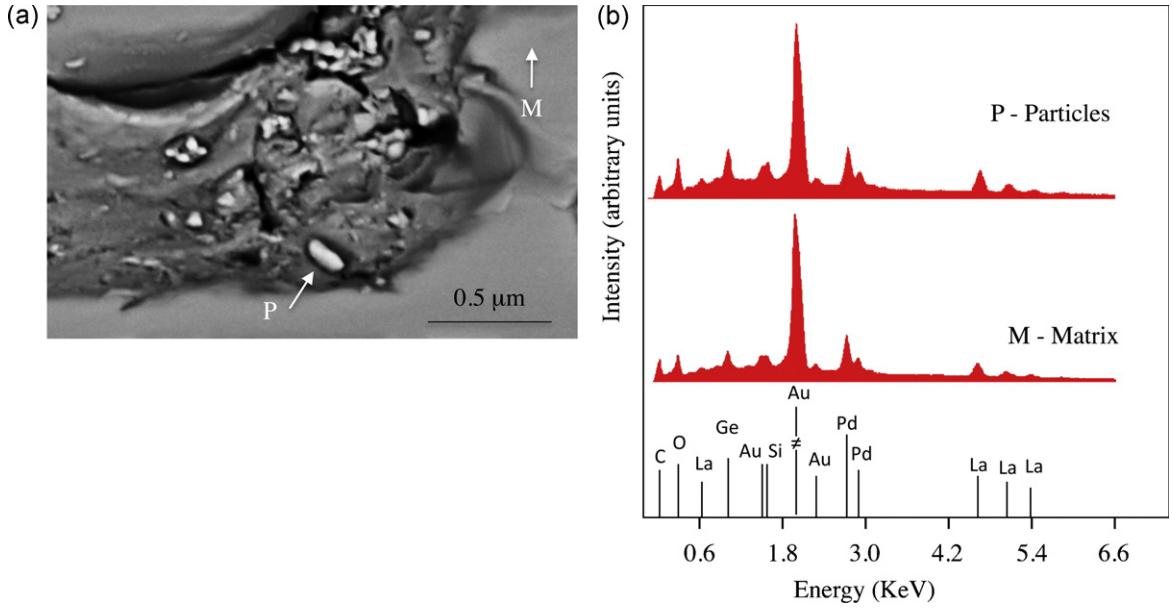


Fig. 5. SEM/EDS of porous area in sample S2: (a) backscattered electron image and (b) EDS spectra of bulk M and loose particle P.

full densification. Loose powder particles can be found in the pores when observed at higher magnification, as shown in Fig. 5(a).

Although different grey levels are seen on the micrograph, which was taken with backscattered electron detector, no significant composition changes were found with EDS point analysis. Indeed, all the spectra exhibit the peaks of the apatite constituent elements, as can be seen on typical spectra of the matrix and loose particles shown in Fig. 5(b). A phase of $La_4GeO_8$ type (without Si) was not detected.

## 4. Conclusions

Oxyapatite-based $La_{9.33}Si_2Ge_4O_{26}$ electrolytes have been prepared by conventional electrical sintering at temperatures ranging from 1300 to 1400 °C in static air for 1 h from dry milling $La_2O_3$, $SiO_2$ and $GeO_2$ powders in a planetary ball mill. The results showed that the apatite phase was formed during milling of all samples, with Ge atoms being incorporated in the Si/Ge-O tetrahedral sites of this phase. Dense samples were obtained by pressureless sintering at 1400 °C, independently of the mechanical alloying conditions used. EDS results showed that the content of germanium in the sintered samples remained almost constant, suggesting that once Ge is incorporated in the apatite phase, its volatilization at temperatures higher than 1250 °C is most likely prevented.

## Acknowledgements

This research is partially sponsored by FEDER funds through the program COMPETE – Programa Operacional Factores de Competitividade and by National funds through FCT – Fundação para a Ciência e a Tecnologia, under the project PTDC/EME-PME/102837/2008. The research fellowships granted to R. Serra and C. Alves are also gratefully acknowledged.

Thanks are also due to Dr. Luís C. Alves and Dr. Alexandra Barreiros for providing the PIXE analysis data obtained at ITN facilities in Sacavém (Portugal).

## References

[1] D.J.L. Brett, A. Atkinson, N.P. Brandon, S.J. Skinner, Intermediate temperature solid oxide fuel cells, Chem. Soc. Rev. 37 (2008) 1568–1578.
[2] Y. Higuchi, M. Sugawara, K. Onishi, M. Sakamoto, S. Nakayama, Oxide ionic conductivities of apatite-type lanthanum silicates and germanates and their possibilities as electrolyte of lower temperature operating SOFC, Ceram. Int. 36 (2010) 955–959.
[3] L. Leon-Reina, E.R. Losilla, M. Martínez-Lara, S. Bruque, M.A.G. Aranda, Interstitial oxygen conduction in lanthanum oxy-apatite electrolytes, J. Mater. Chem. 14 (2004) 1142–1149.
[4] H. Yoshioka, Oxide ionic conductivity of apatite-type lanthanum silicates, J. Alloys Compd. 408–412 (408) (2006) 649–650.
[5] P.J. Panteix, I. Julien, P. Abélard, D. Bernache-Assollant, Influence of porosity on the electrical properties of $La_{9.33}(SiO_4)6O_2$ oxyapatite, Ceram. Int. 34 (2008) 1579–1586.
[6] E. Jothinathan, K. Vanmeensel, J. Vleugels, O. Van der Biest, Powder synthesis, processing and characterization of lanthanum silicates for SOFC applications, J. Alloys Compd. 495 (2010) 552–555.
[7] P.J. Panteix, I. Julien, D. Bernache-Assollant, P. Abélard, Synthesis and characterization of oxide ions conductors with the apatite structure for intermediate temperature SOFC, Mater. Chem. Phys. 95 (2006) 313–320.
[8] L.G. Martínez-González, E. Rodríguez-Reyna, K.J. Moreno, J.I. Escalante-García, A.F. Fuentes, Ionic conductivity of apatite-type rare-earth silicates prepared by mechanical milling, J. Alloys Compd. 476 (2009) 710–714.
[9] H.C. Yao, J.S. Wang, G.G. Hu, J.F. Li, X.R. Lu, Z.J. Li, New approach to develop dense lanthanum silicate oxyapatite sintered ceramics with high conductivity, Solid State Ionics 181 (2010) 41–47.
[10] I. Santacruz, J.M. Porras-Vázquez, E.R. Losilla, M.I. Nieto, R. Moreno, M.A.G. Aranda, Preparation of aluminium lanthanum oxyapatite tapes, $La_{10}AlSi_5O_{26.5}$, by tape casting and reaction sintering, J. Eur. Ceram. Soc. 31 (2011) 1573–1580.
[11] S. Nakayama, M. Sakamoto, M. Higuchi, K. Kodaira, M. Sato, S. Kakita, T. Suzuki, K. Itoh, Oxide ionic conductivity of apatite type $Nd_{9.33}(SiO_4)6O_2$ single crystal, J. Eur. Ceram. Soc. 19 (1999) 507–510.
[12] A. Orera, P.R. Slater, New chemical systems for solid oxide fuel cells, Chem. Mater. 22 (2010) 675–690.

[13] N.H. Menzler, F. Tietz, S. Uhlenbruck, H.P. Buchkremer, D. Stöver, Materials and manufacturing technologies for solid oxide fuel cells, J. Mater. Sci. 45 (2010) 3109–3135.
[14] J.E.H. Sansom, A. Najib, P.R. Slater, Oxide ion conductivity in mixed Si/Ge-based apatite-type systems, Solid State Ionics 175 (2004) 353–355.
[15] E.J. Abram, C.A. Kirk, D.C. Sinclair, A.R. West, Synthesis and characterisation of lanthanum germanate-based apatite phases, Solid State Ionics 176 (2005) 1941–1947.
[16] J.E.H. Sansom, P.R. Slater, Oxide ion conductivity in the mixed Si/Ge apatite-type phases $La_{9.33}Si_{6-x}Ge_xO_{26}$, Solid State Ionics 167 (2004) 23–27.
[17] E. Rodríguez-Reyna, A.F. Fuentes, M. Maczka, J. Hanuza, K. Boulahya, U. Amador, Facile synthesis, characterization and electrical properties of apatite-type lanthanum germanates, Solid State Sciences 8 (2006) 168–177.
[18] A.F. Fuentes, E. Rodríguez-Reyna, L.G. Martínez-González, M. Maczka, J. Hanuza, U. Amador, Room temperature synthesis of apatite-type lanthanum silicates by mechanically milling constituent oxides, Solid State Ionics 177 (2006) 1869–1873.
[19] A.L. Shaula, V.V. Kharton, J.C. Waerenborgh, D.P. Rojas, F.M.B. Marques, Oxygen ionic and electronic transport in apatite ceramics, J. Eur. Ceram. Soc. 25 (2005) 2583–2586.
[20] M.M. Vieira, J.C. Oliveira, A. Cavaleiro, B. Trindade, Mixed Si/Ge apatite-type phase produced by mechanical alloying, Mater. Sci. Forum 587–588 (2008) 128–132.
[21] M.M. Vieira, J.C. Oliveira, A. Cavaleiro, B. Trindade, Synthesis of $La_{9.33}(SiO_4)6O_2$ apatite-type by mechanical alloying, Rev. Adv. Mater. Sci. 18 (2008) 344–348.
[22] R. Serra, C. Alves, J.C. Oliveira, F.A.C. Oliveira, T. Marcelo, J. Mascarenhas, B. Trindade, Synthesis and thermal behavior of $La_{9.33}Si_2Ge_4O_{26}$ apatite for SOFCs, J. Alloys Compd., doi:10.1016/j.jallcom.2011.11.091, in press.
[23] IEC, Standard Publication 672-2, Specification for Ceramic and Glass Insulating Materials. Part 2: Methods of Test, First Edition, Bureau Central de la Commission Electrotechnique Internationale, Genéve, Switzerland, 1980.
[24] L.C. Alves, M.B.H. Breese, E. Alves, A. Paúl, M.R. da Silva, M.F. da Silva, J.C. Soares, Micron-scale analysis of SiC/SiCf composites using the new Lisbon nuclear microprobe, Nucl. Instrum. Meth. B 161–163 (2000) 334–338.
[25] International Centre for Diffraction Data, Powder Diffraction File-2, ICDD, Pennsylvania, 2010, ISSN 1084-3116 [CD-ROM].
[26] B. Li, J. Liu, Y. Hu, Z. Huang, Preparation and characterization of $La_{9.33}Si_6O_{26}$ powders by molten salt method for solid electrolyte application, J. Alloys Compd. 509 (2011) 3172–3176.
[27] S.P. Jiang, L. Zhang, H.Q. He, R.K. Yap, Y. Xiang, Synthesis and characterization of lanthanum silicate apatite by gel-casting route as electrolytes for solid oxide fuel cells, J. Power Sources 189 (2009) 972–981.
[28] S. Beaudet Savignat, A. Lima, C. Barthet, A. Henry, Elaboration and ionic conduction of apatite-type rare earth oxides, Electrochem. Soc. Proc. 2003–07 (2003) 372–378.
[29] J.E.H. Sansom, L. Hildebrandt, P.R. Slater, An investigation of the synthesis and conductivities of La-Ge-O based systems, Ionics 8 (2002) 155–160.
[30] V.V. Kharton, A.L. Shaula, M.V. Patrakeev, J.C. Warenborgh, D.P. Rojas, N.P. Vyshatko, E.V. Tsipis, A.A. Yaremchenko, F.M.B. Marques, Oxygen ionic and electronic transport in apatite-type solid electrolytes, J. Electrochem. Soc. 151 (2004) 1236–1246.